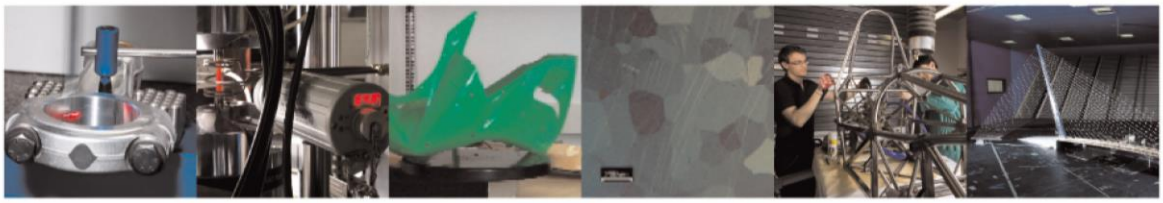

Formability enhancement of Al 6060 sheets through fiber laser heat treatment

Zarini, Stefano; Mostaed, Ehsan; Vedani, Maurizio; Previtali, Barbara

This is a post-peer-review, pre-copyedit version of an article published in INTERNATIONAL JOURNAL OF MATERIAL FORMING. The final authenticated version is available online at: http://dx.doi.org/10.1007/s12289-016-1316-5

1 Introduction

Forming and hydroforming are key technologies in plastic deformation processes for their capability to produce lightweight, structurally stiff and strong pieces characterized by complex shapes. In these manufacturing processes, the initial semifinished component is subjected to a specific strain field with the aim of gradually changing its shape. According to the employed material (aluminum, brass, low alloy steel and stainless steel), the maximum deformation which can be applied to shape the semifinished part is limited to a pre-defined extent, as supplied for instance by the forming limit diagrams. Among the aforementioned materials, aluminum alloys are gathering much attention in numerous fields such as automotive and aerospace due to their low density, good mechanical proprieties and high corrosion resistance [1-3]. Nevertheless, in annealed condition and at room temperature (the usual conditions for forming and hydroforming) aluminum alloys are characterized by lower fracture elongation when compared to stainless steels, low carbon steels and brass [4]. For this reason, in order to obtain complex shapes, intermediate annealing stages are usually introduced during the production cycle.

Among the most common aluminum alloys, the alloy 6xxx is the most employed due to due to its higher ductility and age hardenability.Two are the current limits during the forming and hydroforming of 6xxx aluminum alloy: (i) the limited elongation to failure of the material, (ii) the rapid age hardening of alloys due to the formation of Mg_2Si clusters which obstruct dislocation movement, causing cracking and wrinkling during the forming process [5].The first limitation is overcome by introducing some intermediate annealing heat treatment between deformation steps [6]. On the contrary, the age hardening issue imposes the material to be processed fairly quickly after solution heat treatment in order to avoid Mg_2Si clusters formation and thus material formability reduction.

Nowadays two annealing options during forming and hydroforming are available: the component can be fully annealed or it can be locally heat treated (only a portion of the piece is treated). When the component is fully annealed, heat treatment is generally obtained via furnace heating and a homogeneous temperature field is provided to the full part. On the other hand, in local heat treatments heat is delivered only where it is needed. Since only specific portions of the component are treated (hence softened), the material flow and the inner forces during subsequent deformation will be locally affected. This process produces the so called Tailored Heat Treated Blanks (THTB) [7].

The use of a THTB on large and low thickness components has two advantages: (i) distortion due to stress relieving during the heat treatment in furnaces is much limited [8] (ii) since the thermal energy is provided only to a portion of the component, the consequent energy saving turns immediately in a cost reduction.

In literature and in the industrial practice, three different methods are known to promote local heat treatment: electromagnetic induction, laser radiation, and heat conduction by heated contact plates. When large areas of massive production series need to be treated, electromagnetic induction heating and heating through conduction plate are generally applied [7]. On the contrary, if small or medium areas on complex shaped elements need to be treated, a laser head mounted on a robot arm is the preferred solution. The laser beam indeed gives the advantage to be opportunely shaped both in space and time whilst, the robot arm gives unique flexibility in terms of trajectory planning, avoiding the need to redesign the conduction plate or the heat inductor at each new geometry. Advantages of application of THTB using laser was further proved in [9].

Among the available laser sources, diode and active fiber lasers are nowadays the best candidates in numerous metal processes (not only cutting and welding but also heat treating and cladding) due to their greater reliability, stability and efficiency if compared to CO_2 lasers [10, 11]. Moreover, the short wavelength (729-990 nm for diodes [11] and 1030-1070 nm [10] for fiber laser sources, respectively) is favorably absorbed by the metallic surfaces at solid state [11]. In particular, aluminum alloys present a peak of absorption within the range of diode laser [11]. On the contrary, the absorption at 1 µm (active fiber laser range) is slightly lower [11] whilst at 10.60 µm (CO_2 wavelength) it drops drastically [11]. Moreover, fiber and diode laser beams, differently from the CO_2 ones, can be transmitted through optical fiber, easily handled by cartesian and anthropomorphic systems.

In literature, several research works are reported on local heat treatment of metallic sheets by laser to recover their deformability. Most of them deal with steels for automotive applications. Giorleo et al. [12, 13] proved that CO_2 laser passes applied on strained parts were able to locally decrease the hardness of the material thus enhancing ductility. A similar study was conducted using Nd:YAG on dual phase and martensitic steels in order to increase materials formability [14]. G. Tani et al. [15] presented a mathematical model for predicting mechanical property variation in laser hardening of hypo-eutectoid steels, when the softening effect due to the overlapping trajectories is considered.

One of the first studies aimed at enhancing formability on aluminum using a laser was provided by Vollertsen et al. [16]. The authors demonstrated an increase fracture elongation in homogeneous and inhomogeneous aluminum blanks using a

CO_2 laser. In the paper the aluminum surface was covered with graphite layer in order to increase the absorption at the CO_2 wavelength. Merklein et al. [17] extended the process window in forming 1 mm thick aluminum sheets (series 6xxx) using a Nd:YAG laser. Gaiger et al. [7] further defined the guidelines for the design of THTB made of AlMgSi and ultra-fine grained aluminum. Application of the guidelines for the design of the THTB was used in [18] where a numerical model was implemented to identify the area to be treated to enhance aluminum alloy formability. A different approach is shown in other studies where a laser source was proposed as media for heating up the material during the forming. This process allowed to increase the material flow [19, 20] and thus to reduce cracks. Similar works are also reported elsewhere [21, 22].

In the reported state of the art, two main lacks are observed: (i) fiber laser was never used for local recovery of aluminum THTB (ii) a systematic comparison of mechanical proprieties variation obtained through Furnace Annealing (FA) and Laser Annealing (LA) of pre-deformed aluminum sheets is missing.

In this paper LA making use of a fiber laser source and FA treatment were compared on a EN AW 6060 alloy considering three different response variables: microstructure, micro-hardness and mechanical proprieties evaluated via tensile tests. The level of pre-deformation (namely the strain induced before the annealing) is the controlled variable: low and high deformations were given to sheet samples and the effect of the LA and FA treatment was then investigated. Results deriving from LA treatment are then compared to FA data.

2 Motivation

Critical features to be obtained in hydroforming process are well presented in [23] which offers, in the scheme reported in Figure 1, a significant exemplificative case. The stepped geometry on sides of the part and the local dome on the top in Figure 1 could be the areas where a local heat treatment could bring remarkable advantages in view of a local increase in material formability.

To achieve the aforementioned requirement, in the industrial practice components such as the example in Figure 1 is usually furnace annealed. Alternatively, a laser beam can be locally focused and moved on the critical regions of the component using a 6 arm robot and a scanning system. In addition to the flexibility given by the robot, another important advantage offered by laser is its readiness and immediate availability as heating source, to the point that it can be applied for local intermediate annealing cycles during the various hydroforming steps.

In laser heat treatment processes the thermal cycle is composed by two phases: (i) heating and (ii) cooling stages. Differently from furnace treatments the soaking time is not considered. Due to the movement of the laser beam and to the fast cooling cycles induced by the cold surrounding material in fact, the temperature can be hardly kept constant. Moreover in LA the heating up and the cooling down stages are influenced by numerous parameters, some of them belonging to the laser beam (namely: laser mode, laser power, beam speed, spot diameter), some others belonging to the material and surface (namely: initial level of deformation, thermo-physical proprieties, optical aspect, roughness and possible oxidation or contamination layer of the surface). In addition to these phenomena, two other important aspects must be taken into account. First: after the initial transient, the thermal cycle is not constant along the thickness, second: the cooling cycle can be hardly controlled due to the presence of the bulk material that exerts a heat sink action. For these reasons, the main process parameters such as laser power, laser beam diameter and beam speed have to be opportunely set as a function of the material, surface conditions and level of deformation induced by the hydroforming process to be successfully implemented in a real contest.

Finally, it is also to remark that, due to the small size of the laser beam, is often required to apply a multipass strategy for the achievement of a significant annealing effect. In this case, several adjacent passes have to be performed in order to cover the surface to be treated and the entity of overlapping between adjacent tracks needs to be carefully investigated [24, 25].

In the following work, a pure experimental campaign is presented on EN AW 6060 alloy blanks for both LA and FA treatments. Being the processes dependent from the amount of pre-deformation stored in the material, tests are carried out on cold rolled (CR) blanks work-hardened at different levels. Firstly, proper LA process parameters are identified using a single pass approach, then these are extended to larger areas. The extension to larger areas is tested on different overlapping grades. On the other hand, different soaking times are tested for FA treatment while temperature was fixed to a standard level. The best condition is determined for both treatments (LA and FA) and then effects were compared in terms of feasibility, metallurgical microstructure and mechanical performances.

3 Material and equipment

The material used in this study consisted of fully annealed sheets made of EN AW 6060 alloy with thickness equal to 2 mm. The chemical composition of the investigated alloy is reported in Table 1.

The laser source IPG YLR-1000 (whose characteristics are reported in Table 2) was coupled with an industrial head characterized by a focal length of 200 mm and a collimation length of 100 mm. Nominal waist diameter at focal plane generated by the configuration is 100 µm. The head was mounted onto an industrial robot ABB 2400-10.

To induce predefined levels of plastic deformation into the material, sheet samples were cold rolled to reduction of thisckness of 25 and 50% respectevly. To briefly summarize investigated process conditions, the labels proposed in Table 3 will be used hereafter.

As explained in the motivation section, the LA experimentation consisted of two parts: (i) process parameter identification in case of single pass, (ii) application of identified process parameters at three multi-pass strategies to obtain uniform mechanical proprieties. Selection of the proper process parameters is done evaluating the hardness homogeneity in the treated area: undesired mechanical variation should be avoided.

As far as FA is concerned, soaking time was obtained through a systematic investigation. Finally, configuration which guaranties the best results in terms of microstructure and hardness uniformity of LA samples in multi tracks configuration was compared to the one obtained by the FA treatment. The comparison was also carried out by considering results of tensile tests.

The LA process is described in the rationale scheme of Figure 2. In the scheme the laser head, the laser beam profile and the out of focus configuration needed to increase the treated area are shown.

Single track LA was performed as shown in Figure 3a. Different level of power and speed were tested in order to identify process parameters. Table 4 summarizes fixed and variable process parameters for the two different levels of deformation induced in the material. Range limits of variable parameters were identified through a preliminary experimental campaign here not reported for sake of briefness.

Once the proper set of process parameters was identified in the single track experimentation, the multi track experimentation was performed. With reference to Figure 3b three different configurations were tested:

- 1st configuration: 2 mm interpass distance, overlapped tracks;
- 2nd configuration: 4 mm interpass distance, adjacent tracks;
- 3rd configuration: 6 mm interpass distance, spaced tracks.

The summary of the investigated process parameters is given in Table 5.

In order to evaluate the efficiency of LA as well as to make a proper comparison with a conventional thermal annealing, CR samples were furnace annealed according to the process parameters shown in Table 6.

To assess the quality of both annealing processes, hardness measurement and metallurgical microstructure analysis were performed by cutting the samples along the section A-A represented in Figure 3c. The sections were prepared by standard metallographic techniques including grinding and polishing with a diamond suspension. To reveal the microstructure, electro-etching in Barker's solution at 20 V for 40-90 s was used. Finally samples were observed through OM by polarized light. Assessment of Vickers micro-hardness was conducted according to the standard ASTM E384. 10N load was applied for 15 s. The hardness value reported at each point in the results section is the average of three different measurements (squares in Figure 3c). The spacing between separate tests and minimum distance between an indentation and the edge of the specimen were equal to 2.5 times of the indentation diagonal. Tensile tests were conducted on specimens machined from the treated sheet samples with a gage length of 40 mm at room temperature, with an initial strain rate of 10^{-3} s^{-1}.

4 Results analysis

4.1 Cold rolled materials

Figure 4 shows the typical optical microstructure of SA, CR25 and CR50 samples. As seen in Figure 4a, SA possesses a quite coarse and equiaxed grain structure with average grain size of about 70 µm. The microstructural evolution in CR25 and CR50 sample consists of the progressive generation of elongated grains parallel to the rolling direction (Figure 4b and c).

Characterization of SA, CR25 and CR50 samples is summarized in Table 7. As shown, as the amount of deformation generated by CR increased, the hardness values shifted from 33 to 46 HV and from 33 to and to 50 HV for CR 25 and CR50 samples, respectively.

Figure 5 depicts representative tensile stress versus strain curves for SA, CR25 and CR50 samples. In addition, tensile properties including, yield strength (YS), ultimate tensile strength (UTS) and fracture elongation values are summarized in Table 8. As expected, owing to the work-hardening effect, increasing rolling strain enhances YS and UTS gradually,

but also decreases the uniform elongation significantly. That is, YS and UTS reached 129 and 142 MPa, respectively for the CR50 sample, while elongation to fracture dropped to 3%.

4.2 Fiber Laser Annealing

4.2.1 Single track experimentation

Figure 6a and Figure 6b show effect of different process parameters on different deformation levels of the material. As it can be observed, power greater than 900 W generates melting in CR25LA samples (Figure 6a) while for CR50LA less power was required and it resulted to be also dependent on process speed (Figure 6b).

Figure 7a shows a typical microstructure of a CR25LA sample. As seen, a shallow depth of the sample surface gives evidence that a small volume underwent melting due to the laser radiation. The molten zone is characterized by a columnar grain structure oriented according to main heat flow direction (Figure 7a1). In the heat affected zone (below and next to the molten area) in which process parameters were just below the melting condition, recrystallization followed by grain growth is evident (Figure 7 a2) while in the remaining regions the structure is comparable to that of the original untreated material (Figure 7 a3).

As depicted in Figure 8a and Figure 8b, melting caused an increase in hardness in correspondence of the molten zone. However, in the adjacent zones the decrease of hardness is evident. On the contrary, not only hardness did not increase but rather decreased in the case of process parameter just below melting condition (Figure 8c and Figure 8d) where annealing phenomena effectively occurred. This effect is less evident when the level of deformation is lower (CR25LA) (see Figure 8c vs Figure 8d).

For this reason process parameter representative of Figure 8c and Figure 8d were selected for the multitrack tests. These were: P=650 W and v=3 mm/s for CR50 samples and P=950 W and v=3 mm/s for CR25 samples.

4.2.2 Multi tracks experimentation

Effect of distinct tracks and evidence of their relative distance are evident looking at the microstructures given in Figure 9. In CR50LA samples, for any track interpass distance investigated (2-4-6 mm), recrystallization is more evident with respect to CR25LA samples. This is due to the higher amount of energy stored in the material that results in much higher driving energy for recrystallization. Similarly, the transition zone between base material and treated area is less evident in case of CR25LA samples (Figure 9 a2, c2 and e2 vs Figure 9 b2, d2, f2). It should be noted that, in all configurations the microstructure of CR25LA is always coarser than that of CR50LA in full agreement with accepted recrystallization laws (the higher the stored energy/pre-strain, the smaller the recrystallized grain size).

Considering the case of CR50LA samples, it is clear that interpass distance of 2 mm among subsequent tracks generates a uniform microstructure (Figure 9b). This effect tends to reduce increasing the interpass distance. In the worst case, a clear alternate structure (elongated along with recrystallized grains) is generated (Figure 9f). Compared to the FA treated samples, the laser treated CR25LA and CR50LA samples show a smaller grain structure. This implies that the third stage of grain growth did not take place significantly due to very fast thermal cycles induced by the laser.

Considering Figure 10, it is evident that the process was able to confer uniform hardness reduction for interpass distance of 2 mm (Figure 10a and Figure 10b). This benefit can be achieved also with a larger interpass distance (4 mm) provided that a higher amount of cold working energy is stored in the material (Figure 10d). In case of 6 mm interpass between subsequent tracks, the process was not effective on CR25LA samples (Figure 10e), whilst it was partially for the CR50LA samples where an alternate increase and reduction of hardness was achieved (Figure 10f), which is in good agreement with the microstructural observation shown in Figure 9f. After treatment, for interpass distance of 2 mm of CR25LA samples and for all the investigated cases of CR50LA samples, the hardness was restored down to the initial value (SA samples). Considering that uniform treatment along the section is desired, a minimum interpass distance of 2 mm is therefore required. For this reason, 2 mm was selected as optimal distance between subsequent tracks for the comparison of mechanical proprieties of the FA treatment with those of the LA treatment.

4.3 Furnace annealing

Figure 11 shows the typical optical microstructure of deformed and annealed EN AW 6060 samples according to the various conditions investigated. High temperature annealing readily stimulated recovery and recrystallization of the deformed structure. Therefore, already after FA at 450°C for 5 min, the deformed microstructures for both CR25FA and CR50FA consisted of fully recrystallized grains with equiaxed shape. Figure 11b and Figure 11g clearly show that recrystallized grain size decreases with increasing cold rolling reduction, which is due to strain induced nucleation [12]. Once samples were recrystallized, as annealing time increased, grain growth progressed in both CR25 and CR50 samples.

After 30 min of annealing, grains significantly coarsened in both case as shown in (Figure 11e and Figure 11j). Since the total number of nuclei increased with prior cold work, resulting in a smaller recrystallized grain size as prior cold work is increased, [13], therefore, achieved coarser microstructure was noticeable in CR25FA sample.

Figure 12 reveals the micro-hardness of the CR25FA and CR50FA samples annealed at 450°C for different soaking times. As can be seen in Figure 12, the hardness values for both CR25FA and CR50FA were restored, reaching the SA value, after 5 min at 450°C, which is consistent with the microstructural observation in the previous section. By increasing the annealing time, hardnesses values were almost constant.

According to the data supplied in Figure 11 and 12, it can be concluded that the deformed samples reached full annealing condition already by FA for 5 min at 450°C.

Representative tensile engineering stress–strain curves of CR25FA, CR25LA and CR50FA and CR50LA samples are shown in Figure 13a and Figure 13b respectively. For comparison purpose, also the curves of SA and untreated deformed samples are given in the plot. Both YS and UTS values for all LA treated samples significantly decreased and became close to the initial material condition (SA), while the fracture elongation for CR25LA and CR50LA appreciably increased, which is consistent with microstructural observation and micro-hardness characterization mentioned in previous sections. Quantitative comparison of mechanical proprieties is shown in Figure 14. As seen, compared to cold rolled condition, CR25LA and CR50LA samples elongation improved up to 20 and 19% respectively, implying that LA materials retained their formability. However, LA samples' elongations were slightly lower than those measured for SA and FA samples. The trivial decrement of LA samples compared to FA and SA ones could be related to the smaller grain structure as well as residual stress imposed by fast cooling rate during laser processing.

5 Conclusions

Laser annealing was carried out on EN AW 6060 alloy and then compared to equivalent furnace annealing treatment. Microstructural characterization of laser annealed samples through multi-track approach revealed that for any subsequent track distance, recrystallization occurred. However, in cold rolled samples which were submitted to 50% reduction in thickness and further treated by laser, smaller-size recrystallized grains were formed if compared to laser annealed samples reduced in thickness of 25%. This is attributed to the higher amount of stored energy caused by cold rolling. Among the interpass distance values investigated, 2 mm generated a uniform equiaxed-grain structure. Furthermore, due to the fast laser treatment procedure, laser annealed samples showed smaller grain structure compared to the furnace annealed one. Micro-hardness measurements showed that laser annealing process was able to confer homogeneous hardness reduction for an interpass distance of 2 mm , although this achievement was also achieved by subsequent tracks distance of 4 mm in case of samples reduced in thickness of 50 % and further subjected to laser treatment. Tensile properties of laser annealed and furnace annealed samples indicated that both YS and UTS dramatically decreased to nearly those of the starting condition (annealed samples). The fracture elongation for laser annealed treated samples considerably increased, implying the effectiveness of the annealing laser treatment and suggesting the expected gain in formability. These results demonstrate feasibility of fiber laser annealing as a method to locally anneal small portion of material in large mechanical components.

Acknowledgments

The present investigation was financed under the research project ORIGAMI - Original Advanced Manufacturing for Innovation in metal sheet forming, funded by Regione Lombardia. Moreover the authors wish to thank Alberto Monti for his helpful contribution in carrying out part of the experimental work.

References

1. Hatch JE, Aluminum Association (1984) Aluminum: properties and physical metallurgy. ASM International

2. Vasudevan AK, Doherty RD (2012) Aluminum Alloys--Contemporary Research and Applications: Contemporary Research and Applications. Elsevier

3. Troeger L, Starke E (2000) Microstructural and mechanical characterization of a superplastic 6xxx aluminum alloy. Materials Science and Engineering: A 277:102-113

4. Schneider R, Heine B, Grant R (2014) Mechanical Behaviour of Commercial Aluminium Wrought Alloys at Low Temperatures. Intech, Croatia

5. Kim J, Jeong H, Hong S, Kim Y, Kim W (2001) Effect of aging treatment on heavily deformed microstructure of a 6061 aluminum alloy after equal channel angular pressing. Scr Mater 45:901-907

6. Merklein M, Lechner M, Kuppert A (2012) Enhancement of formability of aluminum alloys in multi-stage forming operations by a local intermediate heat treatment. Production Engineering 6:541-549

7. Geiger M, Merklein M, Vogt U (2009) Aluminum tailored heat treated blanks. Production Engineering 3:401-410

8. Totten GE, Howes MA (1997) Steel heat treatment handbook. CRC Press

9. Merklein M, Geiger M (2002) New materials and production technologies for innovative lightweight constructions. J Mater Process Technol 125:532-536

10. Svelto O, Hanna DC (1998) Principles of lasers

11. Li L (2000) The advances and characteristics of high-power diode laser materials processing. Optics and Lasers in Engineering 34:231-253

12. Giorleo L, Ceretti E, Giardini C, Previtali B (2011) Counter laser treatment for recovering deformation of slender workpiece 473:981-988

13. B. Radhakrishnan, G.B. Sarma, T. Zacharia (1998) Modeling the kinetics and microstructural evolution during static recrystallization—Monte Carlo simulation of recrystallization. Acta Mater 46: 4415–4433

14. Neugebauer R, Scheffler S, Poprawe R, Weisheit A (2009) Local laser heat treatment of ultra high strength steels to improve formability. Production Engineering 3:347-351

15. Tani G, Orazi L, Fortunato A (2008) Prediction of hypo eutectoid steel softening due to tempering phenomena in laser surface hardening. CIRP Annals-Manufacturing Technology 57:209-212

16. F. V, K. L (1998) Enhancement of Drawability by Local Heat Treatment. Annals of the ClRP 47

17. Merklein M, Nguyen H (2010) Advanced laser heat treatment with respect for the application for Tailored Heat Treated Blanks. Physics Procedia 5:233-242

18. Geiger M, Merklein M, Staud D, Kaupper M (2008) An inverse approach to the numerical design of the process sequence of tailored heat treated blanks. Production Engineering 2:15-20

19. Kratky A, Liedl G, Bielak R (2004) Ladd-laser assisted deep drawing. na

20. Bammer F, Schumi T, Otto A, Schuöcker D (2011) Laser assisted bending for efficient light-weightproduction. Technical Gazette 18:571-576

21. Kratky A (2006) Laser assisted forming techniques:634615-634615-11

22. Yoshihara S, MacDonald B, Nishimura H, Yamamoto H, Manabe K (2004) Optimisation of magnesium alloy stamping with local heating and cooling using the finite element method. J Mater Process Technol 153:319-322

23. Vollertsen F (2000) Accuracy in process chains using hydroforming. J Mater Process Technol 103:424-433

24. Gupta A, Lloyd D, Court S (2001) Precipitation hardening in Al–Mg–Si alloys with and without excess Si. Materials Science and Engineering: A 316:11-17

25. Hirth S, Marshall G, Court S, Lloyd D (2001) Effects of Si on the aging behaviour and formability of aluminium alloys based on AA6016. Materials Science and Engineering: A 319:452-456

6 Figures

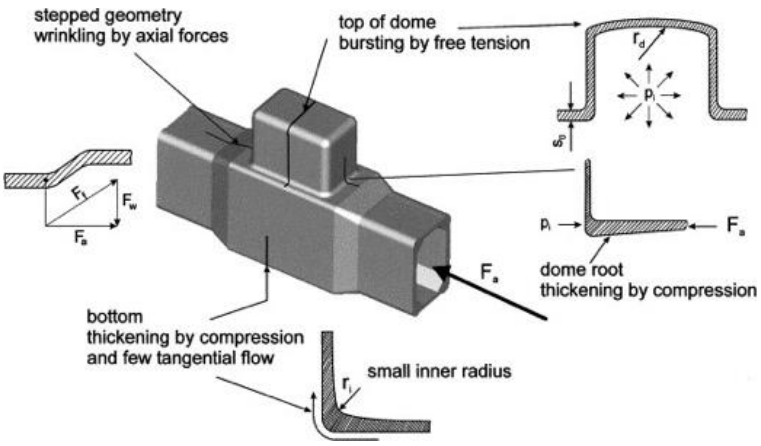

Figure 1: Typical defects of T shaped hydorformed structure[23]

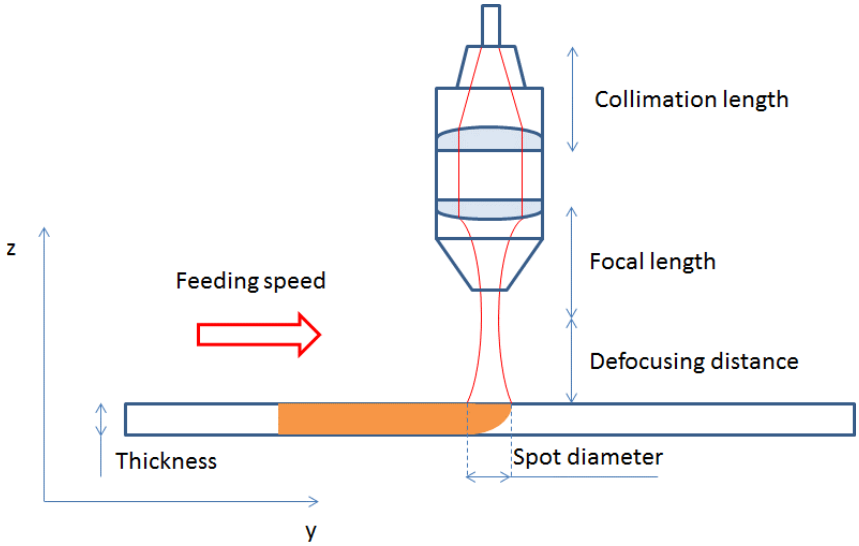

Figure 2: Laser head configuration

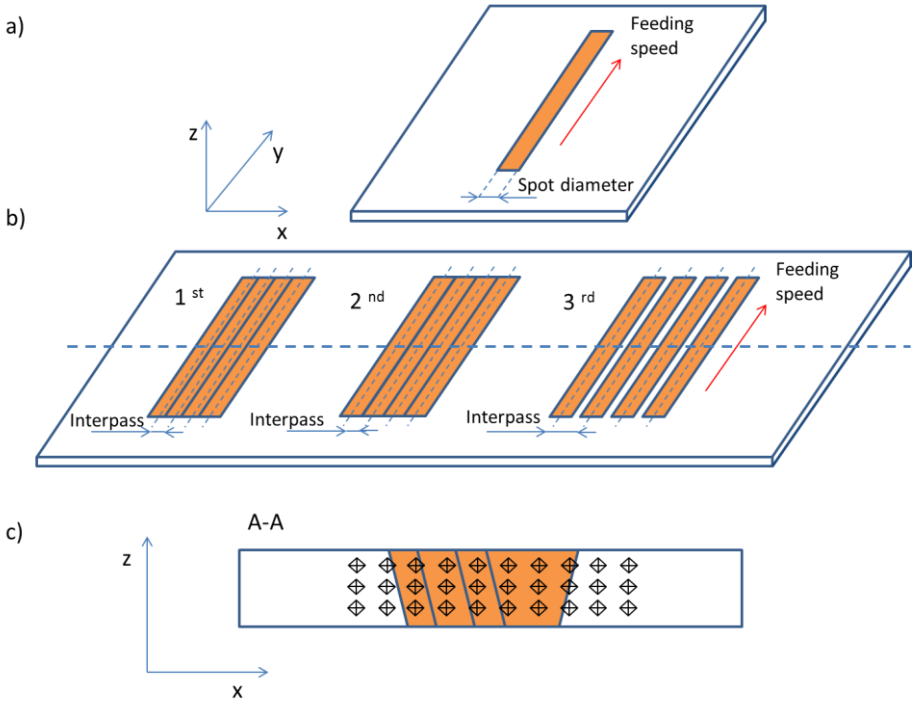

Figure 3: LA: (a) Single track, (b) Multi tracks configurations, Interpass distance of: 1st: 2 mm , 2nd: 4 mm s and 3rd: 6 mm, c) Example of the hardness measurement method in the treated area

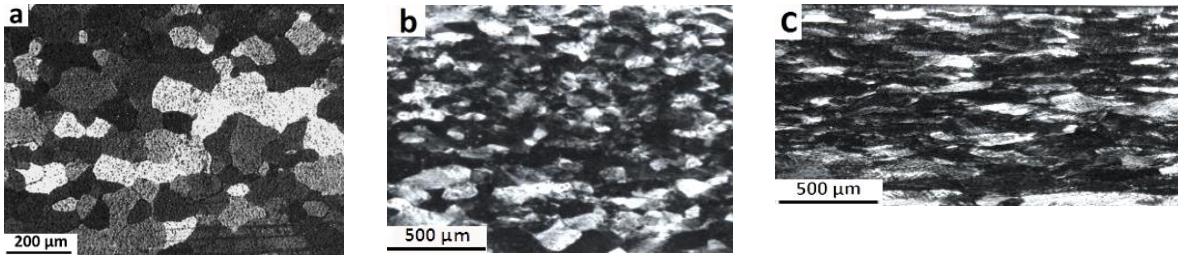

Figure 4: Optical microstructure of the material in (a) SA, (b) CR25 and (c) CR50 conditions

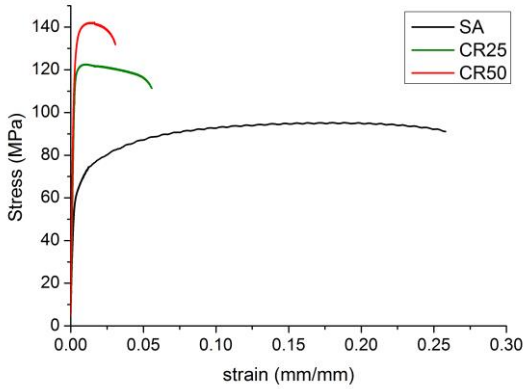

Figure 5: Tensile stress–strain curves measured at room temperature of the SA, CR25 and CR50 samples.

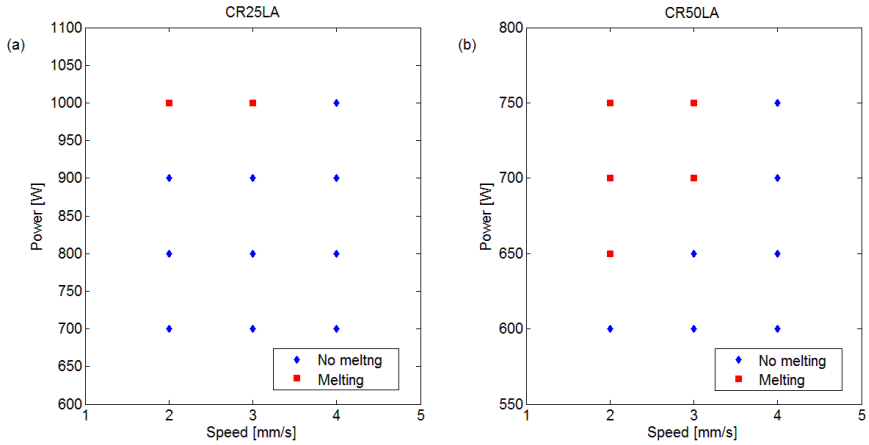

Figure 6: Description of melting/no-melting conditions according to different process parameters. (a) CR25LA (b) CR50LA

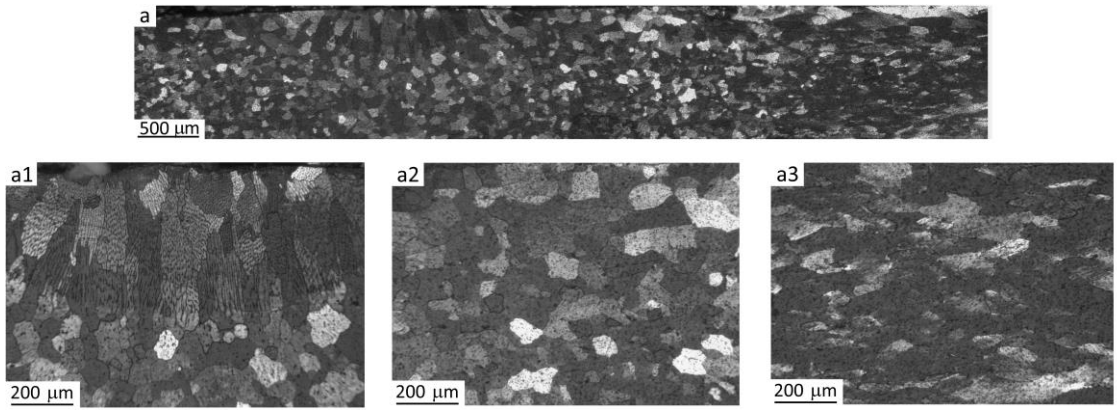

Figure 7: Melting generated with laser on CR25LA samples at P=1000W and v=3mm/s: (a) overview of typical microstructure (a1) magnification of the molten area (a2) magnification of the area surrounding the molten part (a3) elongated grains not affected by the laser heat treatment

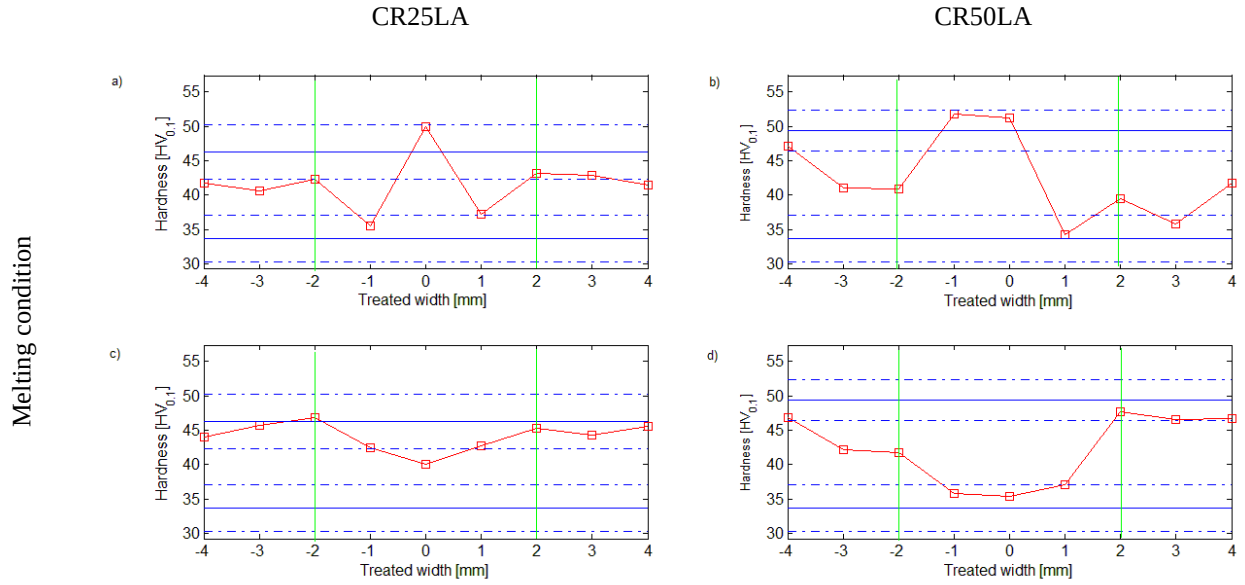

Figure 8: Typical hardness profile of: (a) melting condition in CR25LA samples P=1000W v=3 mm/s, (b) melting condition in CR50LA samples P=700W v=3 mm/s, (c) no-melting condition in CR25LA samples P=900W v=3 mm/s, (d) no-melting condition in CR50LA samples P=650W v=3 mm/s. The upper continuous line identifies the average hardness before laser treatment whilst the dotted lines the scatter bands considering two times the standard deviation. The lower continuous line identifies the hardness of SA sample whilst the dotted lines the scatter bands considering two times the standard deviation. The two vertical lines identifies the area treated by the lasert

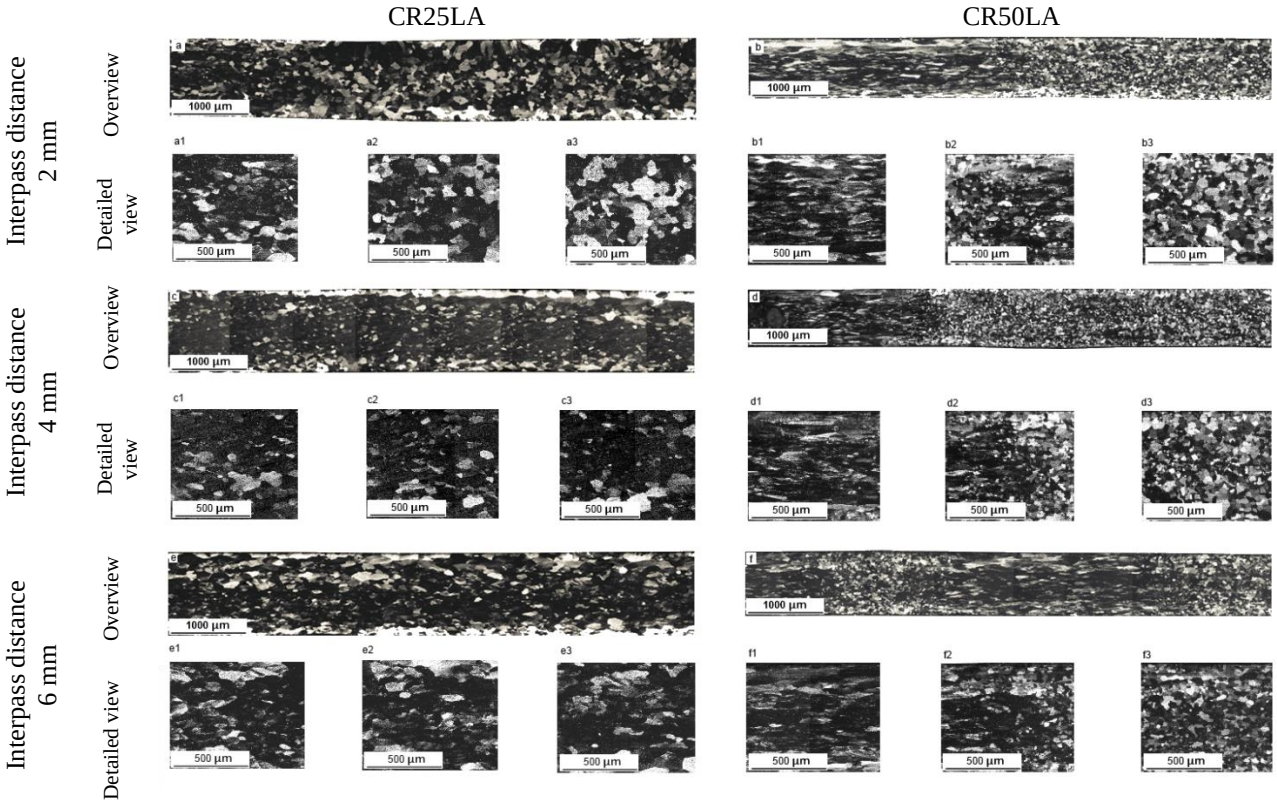

Figure 9: Microstructural development of: (a) CR25LA shift 2 mm (a1) base material (a2) HAZ (a3) annealed area, (b) CR50LA shift 2 mm (b1) base material (b2) HAZ (b3) annealed area, (c) CR25LA shift 4 mm (c1) base material (c2) HAZ (c3) annealed area, (d) CR50LA shift 4 mm (d1) base material (d2) HAZ (d3) annealed area, (e) CR25LA shift 6 mm (e1) base material (e2) HAZ (e3) annealed area, (f) CR50LA shift 6 mm (f1) base material (f2) HAZ (f3) annealed area.

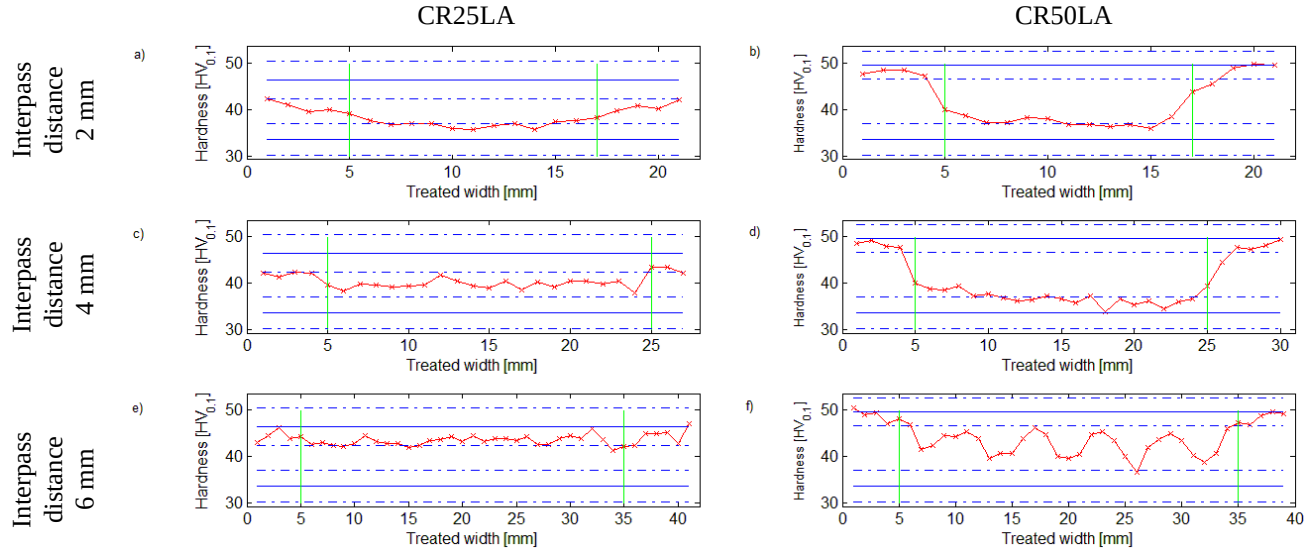

Figure 10: Vickers micro-hardness profiles in: (a) CR25LA shift 2 mm, (b) CR50LA shift 2 mm, (c)CR25LA shift 4 mm, (d) CR50LA shift 4 mm, (e) CR25LA shift 6 mm, (f) CR50LA shift 6 mm. The upper continuous line identifies the average hardness pre-treatment whilst the dotted lines the average plus and minus two times the standard deviation. The lower continuous line identify the hardness of non-cold rolled sample whilst the dotted lines the average plus and minus two times the standard deviation. The two vertical lines identifies the treated by the laser.

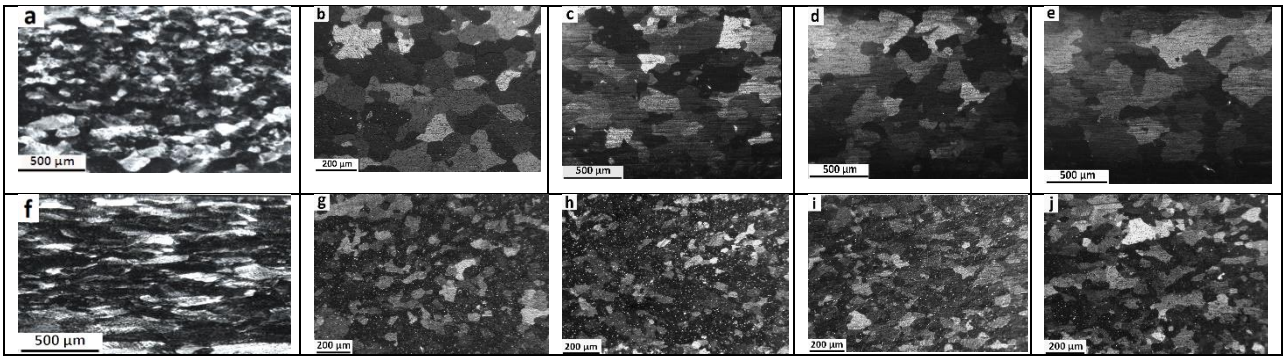

Figure 11: Microstructural evolution of (a) CR25 and (f) CR50 EN AW 6060 alloy during FA at 450˚C for (b, g) 5 min, (c, h) 10 min, (d, i) 15 min and (e, j) 30 min.

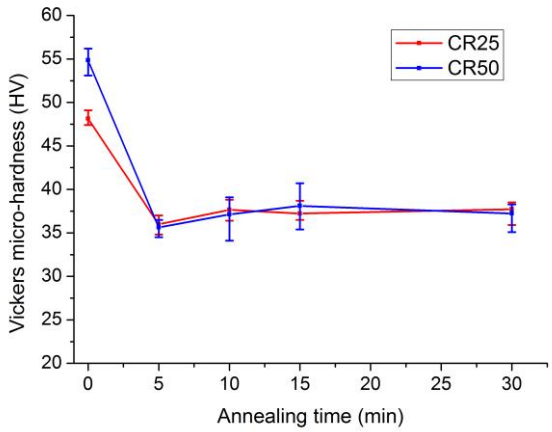

Figure 12: Vickers micro-hardness changes in CR25FA and CR50 FA during different annealing time

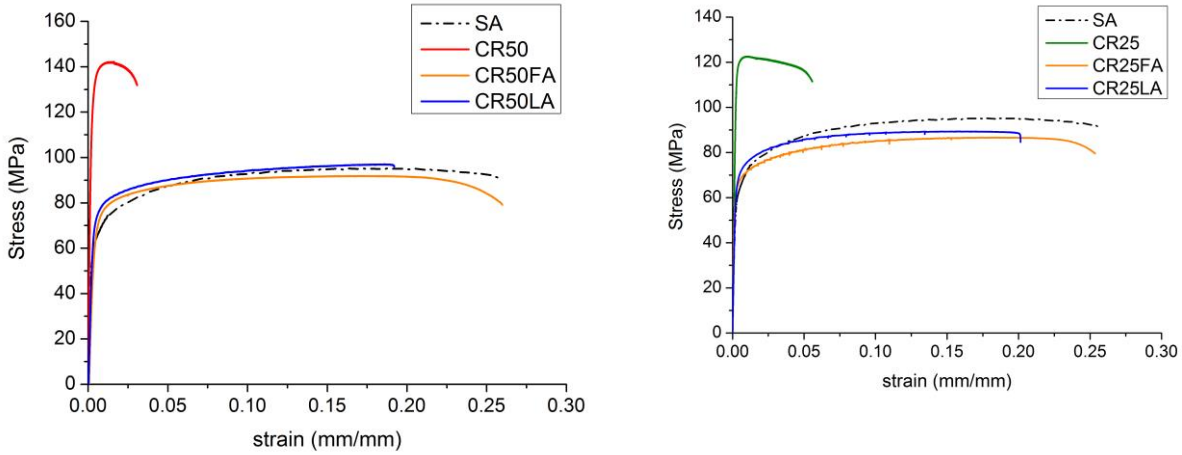

Figure 13:Tensile behavior of: (a) CR25FA and CR25LA samples and (b) CR50FA and CR50LA samples.

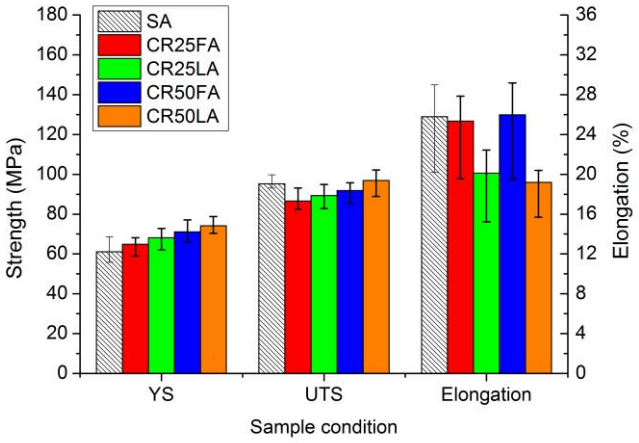

Figure 14: Variation in YS, UTS and fracture elongation in FA and LA treated samples

7 Tables

Table 1: Nominal chemical composition of the investigated EN AW 6060

[wt.%]	Si	Fe	Cu	Mn	Mg	Cr	Zn	Ti
EN AW 6060 alloy	0.45	0.20	<0.001	0.01	0.39	<0.001	0.00	0.02

Table 2: General characteristic of the laser system

Maximum power	1000 W
Wavelength	1070 nm
Fiber core diameter	50 µm
M^2	5.14
Beam waist diameter	100 µm
Focal length	200 mm
Collimation length	100 mm

Table 3: Sample codes used in the paper

Sample code	**Sample condition**
SA	Annealed Sample
CR25	SA + cold rolling to 25% reduction in thickness
CR50	SA + cold rolling to 50% reduction in thickness
CR25FA	CR25 + furnace annealing
CR50FA	CR50 + furnace annealing
CR25LA	CR25 + laser annealing
CR50LA	CR50 + laser annealing

Table 4: Summary of single track LA process parameters applied on CR25 and CR50 samples

	Deformation	
Fixed Factors	**CR25**	**CR50**
Defocusing distance	50 mm	50 mm
Spot diameter	4 mm	4 mm
Variable Factors	**CR25**	**CR50**
Power	700-800-900-1000 W	600-650-700-750 W
Speed	2-3-4 mm/s	2-3-4 mm/s

Table 5: Summary of multi track LA process parameters applied on CR25 and CR50 samples

	Deformation	
Fixed Factors	**CR25**	**CR50**
Defocusing distance	50 mm	50 mm
Spot diameter	4 mm	4 mm
Power	950 W	650 W
Speed	3 mm/s	3 mm/s
Variable Factors	**CR25**	**CR50**
Interpass among subsequent tracks	2-4-6 mm	2-4-6 mm
# of replica	3	3

Table 6: Summary of FA process parameters

Fixed Factors	**Levels**
Soaking temperature	450 °C
Variable Factors	**Levels**

Soaking time	5-10-15-30 min

Table 7: Micro-hardness values achieved for the different cold rolling levels

	Deformation (reduction in thickness)		
Sample condition	SA	CR25	CR50
Vickers micro-hardness [HV]	33 ± 5	46 ±6	50 ± 5

Table 8: Tensile proprieties of the initial conditions for SA, CR25 and CR50 samples

Condition	YS (MPa)	UTS (MPa)	Elongation (%)
SA	61 ± 6.5	95 ± 3.5	26 ± 5
CR25	119 ± 7	123 ± 7	6 ± 1
CR50	129 ± 8	142 ± 5.5	3 ± 1